Journal of Computing and Information Science in Engineering. Received November 25, 2025;
Accepted manuscript posted February 19, 2026. doi:10.1115/1.4071182

A Hybrid Physical Damage Neural Network for Wear Prediction of Self-Lubricating Bearings

Shuo Wang [a], Shichang Du [a,] *, Liang Yan [a], Shanshan Li [b], and Xianmin Chen [b]

[a] National Key Laboratory of Mechanical System and Vibration, School of Mechanical Engineering, Shanghai Jiao Tong University, Shanghai, 200240, China

[b] National Key Laboratory of Strength and Structural Integrity, Xian, Shaanxi, 710065, China

Abstract: Self-lubricating bearings are widely used in aerospace, marine, and other fields due to their excellent performance. Accurate wear prediction for self-lubricating bearings is crucial for ensuring the reliability and safety. However, achieving both physical interpretability and high accuracy in predictive models remains a challenge, as these bearings typically operate under varying load conditions and in high-noise environments. In this paper, a hybrid physical damage neural network is proposed for wear prediction. First, a "physics neuron operator" based on the Archard wear model is designed and embedded into the network to directly compute wear depth. Second, a cumulative damage law is introduced into this operator to quantify the degradation path of the bearing during operation. Finally, the evolution law of wear stages is encoded as a physical constraint in the loss function to compel the network's learning process to follow the true degradation mechanism. To validate the model, a dedicated test platform was built, and a full life-cycle degradation dataset for self-lubricating bearings was collected. Experimental results show that the proposed model significantly outperforms existing methods in prediction accuracy. Furthermore, this paper provides an in-depth analysis of the model's physical interpretability, revealing its internal working mechanism and significantly enhancing its credibility and generalization ability.

Key words: Hybrid Physical Damage Neural Network, Self-lubricating bearing, Physical interpretability, Wear prediction

1.Introduction

Self-lubricating bearings are spherical plain bearings, as shown in Figure 1. Their structure incorporates self-lubricating materials that maintain a continuous lubricating film during operation, eliminating the need for external oil supply systems [1,2]. This characteristic endows the bearings with maintenance-free operation, compact design, environmental friendliness, and contamination resistance, making them widely used in aerospace, heavy marine engineering, and hydraulic engineering applications [3–5].

Journal of Computing and Information Science in Engineering. Received November 25, 2025;
Accepted manuscript posted February 19, 2026. doi:10.1115/1.4071182

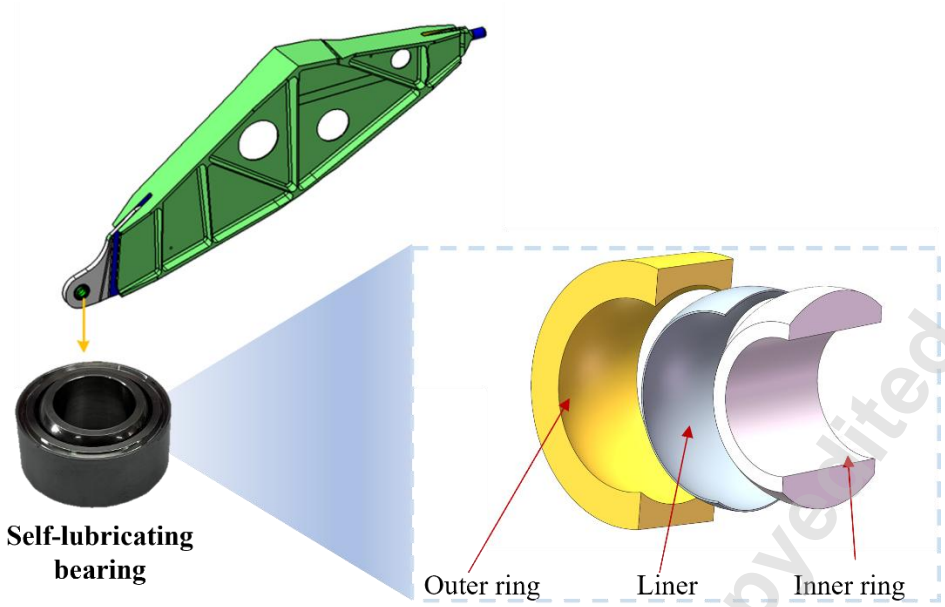

Figure 1. Self-lubricating bearing structure diagram

However, wear is the primary failure mode of self-lubricating bearings [6–9]. Once severe wear occurs, it will directly cause the equipment transmission system to seize up, potentially leading to major safety incidents [10,11]. Severe wear in self-lubricating bearings is illustrated in Figure 2. Therefore, accurately predicting the wear depth of self-lubricating bearings is crucial for real-time assessment of their condition and timely maintenance.

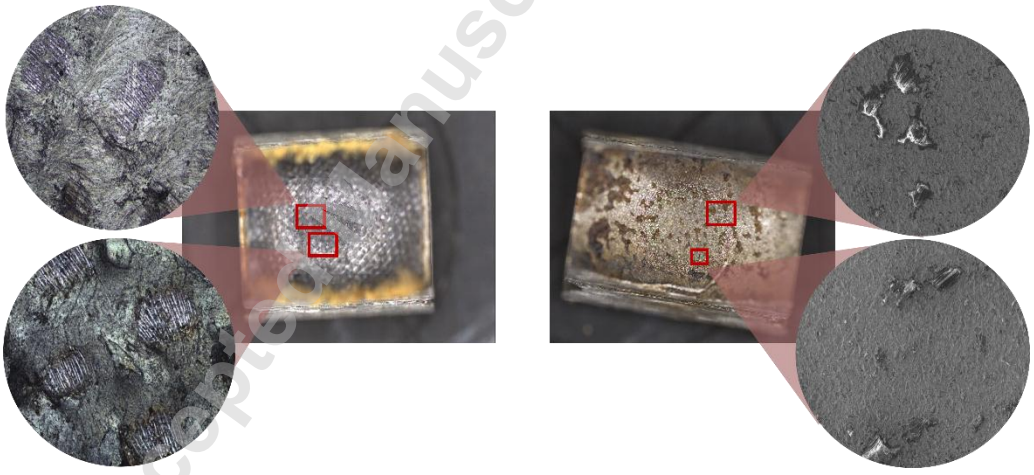

(*a*) New self-lubricating bearing (b) Severe wear

Figure 2. Comparison of before and after wear

Current research on wear prediction falls into three categories: (i) physics-based models, (ii) data-driven models, and (iii) hybrid physical mechanism and data models. The first, physics-based models, are dedicated to predicting wear from first principles by constructing mathematical models that embody the underlying tribological mechanisms. These models (such as the classic Archard model) exhibit excellent

Journal of Computing and Information Science in Engineering. Received November 25, 2025;
Accepted manuscript posted February 19, 2026. doi:10.1115/1.4071182

physical interpretability. However, their predictive accuracy is highly dependent on the precise characterization of contact mechanics, material properties, and wear coefficients. Under actual variable operating conditions (such as load and temperature fluctuations), these parameters are often difficult to obtain accurately. To address this challenge, extensive research has focused on developing high-fidelity physics-based models tailored for specific applications. For instance, Lin et al. [12] developed a dynamics model based on the equivalent load method and integrated it with the Archard model for wear prediction. Xing et al. [13] focused on the change rule of wear, establishing a predictive model for cumulative wear depth and analyzing the influence of axial load on key parameters. Zhang et al. [14] introduced a discretization strategy to characterize the spatial non-uniformity of wear distribution. Li et al. [15] performed more refined modeling of erosion-wear mechanisms. For self-lubricating bearings, Luo et al. [16] conducted high-accuracy numerical simulations of bearing contact and wear behavior using the finite element method. While Lu [17]and Zhang [5] proposed a simplified analytical model based on the "conservation of total wear volume" assumption to reduce computational cost while maintaining accuracy. Hao et al. [18] and Li et al. [19] employed statistical models to fit and extrapolate measured wear degradation data, thereby enhancing the engineering applicability of wear prediction.

Physics-based models rely on precise prior knowledge and idealized assumptions [20,21], which limits their use and reduces prediction accuracy under variable operating conditions. As a countermeasure, the data-driven prediction paradigm has emerged [22–25]. This paradigm treats the physical system as a whole, learning the non-linear mapping between historical monitoring data and wear states to predict future wear [26,27]. The powerful representation capabilities of deep learning models have made them a mainstream technology in this field, such as Multi-layer Perceptrons (MLP), Long Short-Term Memory (LSTM), Deep Neural Networks (DNN), and Convolutional Neural Networks (CNN). Scholars have also conducted in-depth explorations targeting specific engineering problems. For instance, Yau et al. [28] designed an automatic hyperparameter optimizer for artificial neural networks. Liu et al. [29] explored a hybrid forecasting approach combining cluster analysis with machine learning models. Cheng et al. [30] proposed a multi-signal forecasting network integrating Gramian angular fields and residual transform neural networks. Dong et al. [31] constructed a multi-model ensemble framework to handle massive signal volumes. Applications in the field of self-lubricating bearings remain in the early exploratory stages, with a few

representative works including: Pandiyan et al. [32] applied LSTM encoder-decoders to predict bearing wear time series. Hao et al. conducted specialized studies on bearing wear under specific operating conditions such as heavy loads [33] and high-frequency oscillations [34].

Although existing methods have achieved certain progress, developing a wear prediction model that simultaneously possesses high accuracy, strong generalization, and physical interpretability remains a significant challenge [35]. On the one hand, physics-based models are difficult to construct and costly due to their reliance on extensive prior knowledge and experimental data [36]. On the other hand, data-driven approaches are “black-box” models that suffer from issues with physical interpretability [35,37,38]. Furthermore, their performance heavily depends on the quality and quantity of training data [39], often resulting in poor generalization capabilities and high computational costs under scenarios with small samples or multiple variable conditions. Physics-Informed Neural Network (PINN), which combine the advantages of both approaches, have the potential to address the aforementioned challenges [40]. Consequently, PINN is considered a promising method for wear prediction, and some scholars have begun to explore its potential. For example, Pashmforoush et al. [41] and Li et al. [42] enhanced model interpretability by explicitly incorporating physical equation parameters into data-driven models. Gao et al. [43] utilized physical prior knowledge to assist data feature extraction and model construction, thereby improving the consistency between features and actual wear mechanisms. Yuan et al. [44] and Zeng et al. [45] employed data-driven methods to calibrate and optimize unknown or difficult-to-measure parameters in physical models, achieving data assimilation and adaptive correction of physical models. Regarding model fusion strategies, Huang et al. [46] perform weighted fusion of predictions from physical and data models at the output layer using particle filtering to balance stability and accuracy. In contrast, Wang et al. [47] achieve interactive coupling between physical and data-driven features at the intermediate model layer, constructing a more tightly integrated deep fusion hybrid prediction framework.

In fact, constraining data-driven models with physical models can largely address the "black-box" problem and reduce the dependency on data quality. Essentially, this approach replaces a portion of the data-driven model with physical equations, compelling it to learn in accordance with real-world physical laws. However, due to significant challenges in modeling physical behavior under varying operating

conditions and constructing a fusion framework, coupled with the low signal-to-noise ratio of self-lubricating bearing data throughout its entire lifecycle, few researchers have employed hybrid methods for wear prediction under such conditions. Nevertheless, as many recent review papers have pointed out [40,48,49], hybrid methods are a subject worthy of in-depth investigation and are poised to bring tremendous value to the application of artificial intelligence in industry.

This paper proposes a PINN for predicting wear in self-lubricating bearings. This model achieves a true integration of wear laws and neural networks, yielding stable and accurate wear prediction results. Specifically, first, data subsampling is performed using compressive sensing techniques. Second, self-lubricating bearing wear is modeled from the perspectives of degradation patterns and damage. The Archard mechanism and cumulative damage law are designed as “physics neuron operator” to enable wear prediction. Finally, the evolution pattern of wear stages is encoded as a physical constraint within the loss function, compelling the neural network's learning process to adhere to the actual degradation mechanism and guiding the training of the deep learning model. Validation on a dedicated experimental platform demonstrates that the proposed model significantly outperforms existing methods in prediction accuracy.

The main contributions are summarized as follows:

1) A novel “physics neuron operator” was designed. By linking physical damage with wear, the wear prediction framework is constrained within the Archard model, enhancing the model's sensitivity to data and prediction accuracy.

2) A novel physical loss function was designed. This enables the model to adhere to macroscopic degradation patterns without overfitting to local data points, effectively enhancing its generalization capability.

3) Degradation trajectories were designed based on cumulative damage theory. Utilizing cumulative damage values to describe the degradation process of bearings provides theoretical assurance for wear process prediction and enhances the model's physical interpretability.

The rest of this paper is organized as follows. In Section 2, the foundation is formally introduced. In Section 3, details of the proposed model are described. After that, experimental research on the wear degradation of self-lubricating bearings is conducted and the comparative results are presented in Section 4. Finally, conclusions are provided in Section 5.

Journal of Computing and Information Science in Engineering. Received November 25, 2025;
Accepted manuscript posted February 19, 2026. doi:10.1115/1.4071182

2. Theoretical background

2.1 Data downsampling of wear degradation

Downsampling, as a preprocessing technique, aims to mitigate the trade-off between data fidelity and computational efficiency. Its core objective is to compress raw data to a more manageable scale while preserving as much information as possible required for condition assessment. This ensures the efficiency and computational feasibility of subsequent feature extraction and health prediction modeling processes. Given that signal acquisition frequencies must satisfy the Nyquist-Shannon sampling theorem [50], this method is particularly well-suited for preprocessing monitoring signals with inherent high-frequency characteristics, such as acoustic emission (AE) signals.

The theory of Compressed Sensing, proposed by Candes et al. [51], provides a fundamental mathematical framework for circumventing the limitations of the Nyquist sampling theorem. Its core idea is that if a signal $\mathbf{X} \in \mathbb{R}^n$ is sparse in some transform domain, it can be sampled at a rate significantly below the Nyquist rate through non-adaptive measurements using a sensing matrix $\mathbf{\Phi} \in \mathbb{R}^{m \times n}$ that is incoherent with the transform basis. This process linearly projects the high-dimensional signal $\mathbf{X}$ onto a low-dimensional measurement vector $\mathbf{Y} \in \mathbb{R}^m$, where the compression ratio is high ($n >> m$). The essence of this process is that each element in the measurement vector $\mathbf{Y}$ contains global information from the original signal $\mathbf{X}$, which theoretically guarantees that the original high-dimensional signal can be reconstructed exactly or with high probability from these low-dimensional measurements. This fundamentally avoids the aliasing distortion caused by conventional downsampling. The measurement model of compressed sensing can be expressed as follows:

$$\mathbf{X} = \sum_{i=1}^{n} \boldsymbol{\theta}_i \boldsymbol{\psi}_i = \boldsymbol{\Psi}\boldsymbol{\theta} \tag{1}$$

$$\mathbf{Y} = \boldsymbol{\Phi}\mathbf{X} = \boldsymbol{\Phi}\boldsymbol{\Psi}\boldsymbol{\theta} \tag{2}$$

As can be found in [52], the frequency band of AE signals generated during wear monitoring is sparse. Therefore, the Fourier Transform is used here to convert the signal from a non-sparse signal to a sparse one. The formula for the Fourier Transform can be expressed as follows:

Journal of Computing and Information Science in Engineering. Received November 25, 2025;
Accepted manuscript posted February 19, 2026. doi:10.1115/1.4071182

$$\hat{x}[k] = \sum_{n=0}^{N-1} e^{-i\frac{2\pi}{N}nk} x[n] \qquad k = 0,1,\dots,N-1 \tag{3}$$

where x is the high-dimensional signal e is the base of the natural logarithm and i is the imaginary unit. This transformation is usually denoted by the symbol $\mathcal{F}$, i.e.:

$$\hat{x} = \mathcal{F}x \tag{4}$$

Therefore, the sparse matrix $\boldsymbol{\Psi}$ in equation (2) is represented by the Fourier Transform matrix, $\mathcal{F}$. The overall framework of compressed sensing is illustrated in Figure 3.

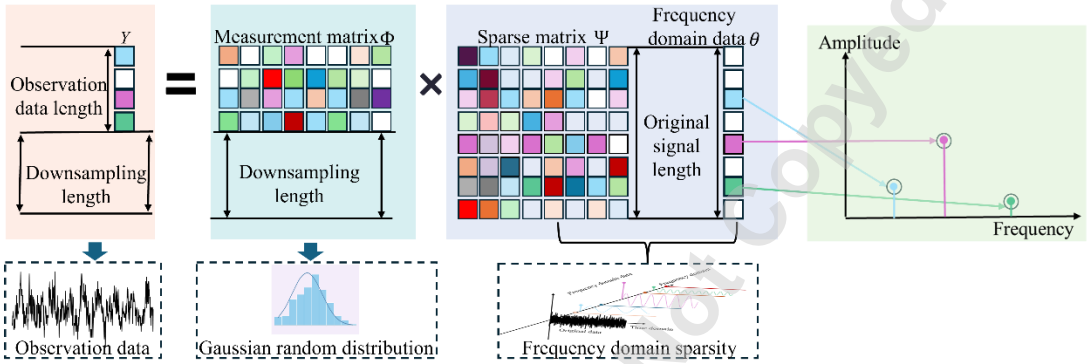

Figure 3. Compressed sensing framework

2.2 Wear degradation law of self-lubricating bearing

The entire life cycle of self-lubricating bearings is typically divided into three classic stages: an initial running-in stage, a steady-state wear stage, and a severe wear stage [53–55], as illustrated in Figure 4. The initial running-in stage exhibits a high wear rate. This is mainly attributed to initial macro-geometrical errors and micro-roughness on the surfaces of the tribo-pair, which lead to a small real contact area and high stress concentration. During this stage, intense interlocking, shearing, and plastic deformation occur between surface asperities, inducing rapid material removal [53,56,57]. However, this seemingly destructive process is, in essence, a constructive surface-flattening mechanism. Under the combined effects of micro-cutting, plastic flow of material, and diffusion of lubricant to the surface layer, the original surface topography is gradually modified. Ultimately, this stage fulfills its core mission: to form a smooth, conformal contact interface, thereby creating the necessary conditions for establishing an effective self-lubricating film and transitioning to the long and gentle steady-state wear phase.

Journal of Computing and Information Science in Engineering. Received November 25, 2025;
Accepted manuscript posted February 19, 2026. doi:10.1115/1.4071182

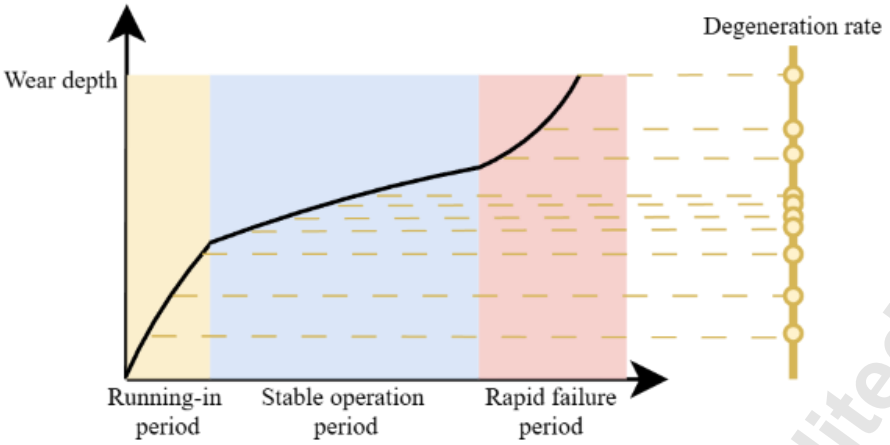

Figure 4. Wear degradation law of self-lubricating bearing

After the running-in period, the bearing enters the steady-state wear stage. At this stage, a uniform and continuous self-lubricating film has formed on the friction pair surfaces, fully utilizing the properties of the lubricant. Consequently, the wear rate decreases significantly and is maintained at a low and relatively constant level, and the tribological performance reaches its optimal state [56,57]. During this stage, the dominant wear mechanisms shift to the more moderate adhesive wear and mild abrasive wear. Due to the extremely low wear rate, the bearing can maintain reliable operation for a prolonged period, exhibiting excellent service durability [53,55]. Therefore, the steady-state wear stage is the longest phase in the life cycle of a self-lubricating bearing, and its duration directly determines the bearing's effective service life and long-term performance.

Ultimately, self-lubricating bearings inevitably transition from steady-state degradation to a catastrophic stage of severe wear due to lubricant depletion or material damage reaching a critical threshold. This stage marks the end of the bearing's functional life. The fundamental cause lies in the compromised integrity of the self-lubricating film, which can no longer effectively isolate the surfaces of the friction pair, leading to direct contact between the metal substrates. Once this stage is entered, the system will experience a positive-feedback, runaway degradation process: the wear rate no longer increases linearly but instead surges exponentially [53–55]. The dominant damage modes shift to highly destructive large-scale spalling, surface delamination, and secondary damage from wear debris. These damages significantly shorten the bearing's remaining useful life and jeopardize its operational safety.

2.3 Recurrent neural network (RNN)

A RNN is a class of artificial neural network architecture specifically designed for

processing sequence data or time-series data. Unlike traditional Feedforward Neural Networks, RNNs introduce recurrent connections into their network structure. This enables the network to utilize hidden states between time steps, thereby effectively capturing temporal correlations and dynamic features within the input data [58]. Specifically, the hidden layer unit in an RNN at each time step receives not only the current input signal but also the output from the previous time step's hidden layer as an additional input; this mechanism enables the network's "memory" function. Through this recursive transmission of the hidden state, an RNN can preserve and update information about the historical sequence within the network. This significantly enhances its ability to handle problems involving temporal dependencies, enabling the dynamic modeling and representation of the temporal information in the input sequence. The mathematical formulation of an RNN is expressed as follows [59]:

$$h_t = \sigma(Wx_t + Uh_{t-1} + b) \tag{5}$$

where $x_t \in \mathbb{R}^M$ and $h_t \in \mathbb{R}^N$ are respectively the input and the hidden state of the cell in a time t. $W \in \mathbb{R}^{N\times M}$ and $U \in \mathbb{R}^{N\times N}$ are the weight matrices of the input of the current cell and the weight matrices of the recurrent input and $b \in \mathbb{R}^N$ denotes the bias of the neuron. $\sigma(\cdot)$ is the activation function of the neuron (sigmoid function).

In the specific task of wear prediction, the architectural advantages of RNNs are fully demonstrated. Wear itself is a cumulative damage process with strong path dependency, meaning the current state is the result of its entire historical evolution. The unique recurrent structure of an RNN, through its recursively updated hidden state, naturally aligns with this physical essence. Specifically, an RNN continuously encodes and compresses historical degradation information and fuses it with new observational data acquired at the current moment. This mechanism of continuous information flow and updates enables the RNN to potentially capture both short-term fluctuation characteristics and long-term evolutionary trends in the wear degradation process. Therefore, an RNN can construct a non-linear dynamic degradation model that more closely reflects physical reality, which is crucial for accurately predicting the future wear trajectory.

3. The Proposed Methodology

The proposed hybrid physical damage neural network framework is illustrated in Figure 5. This framework primarily consists of three steps, briefly described as follows:

1) Data subsampling based on compressed sensing. Compressed sensing

Journal of Computing and Information Science in Engineering. Received November 25, 2025;
Accepted manuscript posted February 19, 2026. doi:10.1115/1.4071182

techniques are employed to subsample the raw acquired signals, compressing the input data to a more manageable dimensionality.

2) Wear calculation based on the Archard model. The subsampled data is fed into a multilayer perceptron to estimate the contact stress at the current time step. Subsequently, the corresponding instantaneous wear depth is computed through the "physics neuron operator" embedded in the Archard model, enabling explicit representation of the wear mechanism.

3) Deterioration trajectory calculation based on the cumulative damage model. Leveraging the sequential memory capability of RNNs, historical wear data is temporally coupled with the current instantaneous wear rate to construct the cumulative damage process. This achieves prediction of the deterioration trajectory throughout the entire life cycle of the self-lubricating bearing.

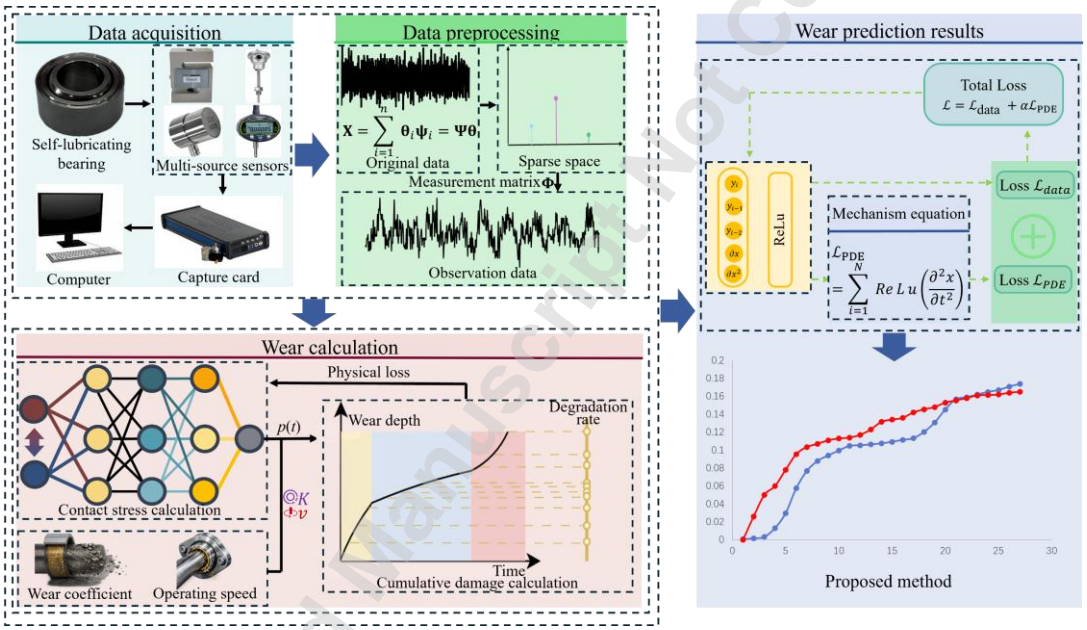

Figure 5. Architecture of the proposed hybrid physical damage neural network

3.1 Self-lubricating bearing wear modeling

The purpose of a PINN is to endow a neural network with strong interpretability and enable it to learn in accordance with physical laws. To ensure that proposed prediction model possesses strong interpretability and generalization capabilities, this paper models the most critical aspect of the wear prediction process: the wear degradation. First, define the damage caused to bearings by external loads. Its mathematical formula can be expressed as follows:

$$D_f = \frac{1}{N_f} \tag{6}$$

where D_f is the damage of self-lubricating bearings, N_f is the life of self-lubricating bearings.

Therefore, the damage to the self-lubricating liner caused by the external load over a time step Δt can be expressed as follows:

$$D_i = \frac{\Delta t}{N_{f,i}} \tag{7}$$

where D_i is the damage of self-lubricating bearing over a time step Δt under ith loading, $N_{f,i}$ is the life of self-lubricating bearings under the corresponding number of load cycles and applied external load.

After a period of operation, the cumulative damage suffered by the self-lubricating bearing can be expressed as follows:

$$D = \sum \frac{\Delta t}{N_{f,i}} \tag{8}$$

where D is the cumulative damage to self-lubricating bearings.

Since the load on the self-lubricating bearing is not a horizontal load and the action between the loads is discrete, equation (8) can be expressed as follows:

$$D = \sum_{i=1}^{n} \frac{N_i}{N_{f,i}} \tag{9}$$

where N_i is the ith number of cycles loaded.

Next, the wear degradation of self-lubricating bearing is defined. Generally, the wear degradation trajectory of self-lubricating bearing is related not only to operating time but also to external load, material hardness, operating speed, and other factors. Therefore, it is proposed to model it as a multivariate function:

$$u = f(t, \mathbf{x}) \tag{10}$$

where t represents time and $\mathbf{x}$ represents a vector composed of external load, material hardness, operating speed, and other factors.

Then, the wear degradation rate of self-lubricating bearings can be expressed as follows:

$$\frac{\partial u}{\partial t} = \varphi\,(t, \mathbf{x}, u; \lambda) \tag{11}$$

The above equation is an explicit partial differential equation parameterized by λ, and $\varphi(\cdot)$ represents the nonlinear function of t, $\mathbf{x}$, and u. The function $\varphi(\cdot)$ characterizes the internal degradation of the self-lubricating bearings, and by altering this nonlinear function, various forms of degradation can be represented.

Journal of Computing and Information Science in Engineering. Received November 25, 2025;
Accepted manuscript posted February 19, 2026. doi:10.1115/1.4071182

For the wear of self-lubricating liner, the wear degradation rate of self-lubricating bearing can be characterized by Archard model [17]. The expression of wear degradation rate and time can be expressed as follows:

$$\gamma = \frac{dh}{dt} = KPv \tag{12}$$

$$\Delta h = KPv\Delta t \tag{13}$$

where γ is the wear rate, h is the wear depth, K is the wear coefficient, P is the contact stress, v is the running speed, Δh is the cumulative depth of wear over a time step Δt.

The data collected by sensors are stage jumping, and it is difficult to collect continuous wear labels. Therefore, the constructed prediction model forecasts wear under a certain time step.

$$\Delta h_i = \Delta N K p_i v_i \Delta t_i \tag{14}$$

where ΔN is the time step, and the rest of the variables are physical meanings corresponding to the ith load.

Since the main failure mode of self-lubricating liner is wear [6–9], the wear degradation of self-lubricating bearing can be equated to the damage suffered by the bearing. Therefore, it is considered that damage to self-lubricating bearing caused by external loads over a time step Δt_i can be expressed as follows:

$$D_i = \frac{\Delta t_i}{N_i} = \Delta N K p_i v_i \Delta t_i \tag{15}$$

Based on the cumulative damage rule of equation (9), the cumulative damage of the bearing at the current moment can be expressed as follows:

$$D = \sum \Delta N K p_i v_i \Delta t_i \tag{16}$$

3.2 PINN Construction

The contact stress established based on prior knowledge in equations (12) and (13) is difficult to solve. It is well known that neural networks are powerful function approximators. Therefore, this paper utilizes the strong approximation capability of neural networks to approximate the contact stress. Combined with equation (16), a "physical neuron operator" for recurrent RNN unit is constructed. Its framework schematic is shown in Figure 6.

Journal of Computing and Information Science in Engineering. Received November 25, 2025;
Accepted manuscript posted February 19, 2026. doi:10.1115/1.4071182

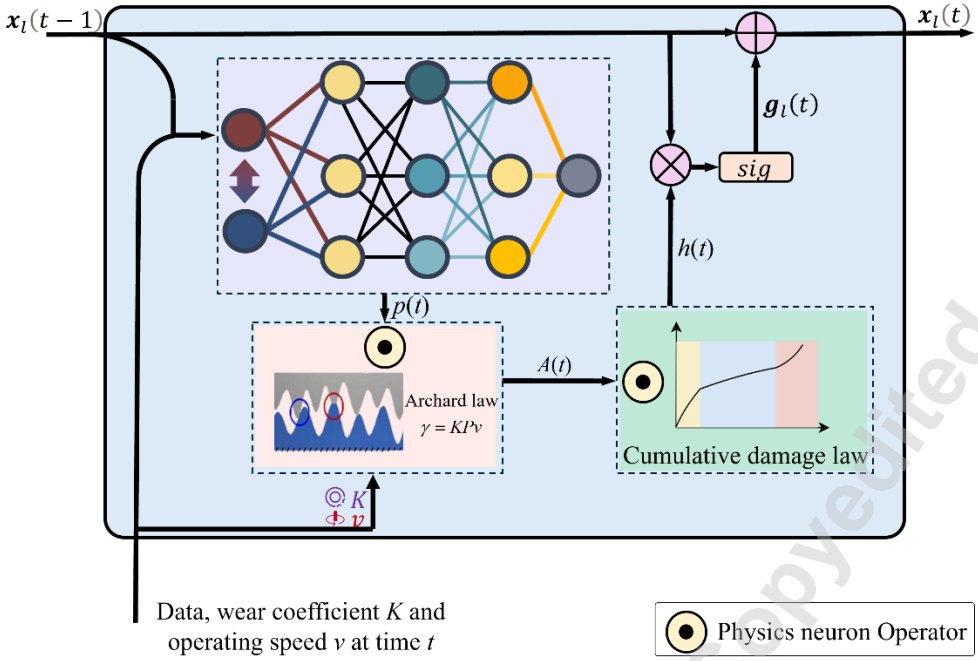

Figure 6. Physics neuron operator structure diagram

Based on the bearing wear conditions defined by the cumulative damage law in Section 3.1 and the time sequence data, this paper defines the wear failure path of the bearing as follows:

$$\boldsymbol{x}_l(t) = \boldsymbol{x}_l(t-1) + \boldsymbol{g}_l(t) + \boldsymbol{\varepsilon}_l(t) \tag{17}$$

where, $\boldsymbol{x}_l(t)$ is the cumulative damage state of self-lubricating bearing at the present time, $\boldsymbol{x}_l(t-1)$ is the cumulative damage state of self-lubricating bearing at last time, $\boldsymbol{g}_l(t)$ is the damage state of the self-lubricating bearing at the present time, $\boldsymbol{\varepsilon}_l(t)$ is environmental noise. For the damage evolution of self-lubricating bearings, a degradation model based on RNN to represent it. The expression is as follows:

$$\boldsymbol{g}_l(t) = \sigma(Wh(t) + U\boldsymbol{x}_l(t-1) + b) \tag{18}$$

where $h(t)$ is the output of the "physics neuron operator" operator in the RNN network, combined with the physical damage operator (16) of section3.1, the physical neural network can be defined as follows:

$$h(t) = \Delta NKp(t)v\Delta t \tag{19}$$

where $p(t)$ is the output of the MLP in the RNN network. So the calculated wear depth for the RNN network can be represented by $A(t)$.

$$A(t) = Kp(t)v\Delta t \tag{20}$$

Since the physical equations constructed are discrete, the degradation trajectories between discrete points are expressed as follows:

Journal of Computing and Information Science in Engineering. Received November 25, 2025;
Accepted manuscript posted February 19, 2026. doi:10.1115/1.4071182

$$\boldsymbol{x}_l(t+\Delta n) = \big(\boldsymbol{x}_l(t+1) - \boldsymbol{x}_l(t)\big)/\Delta n \tag{21}$$

where Δn is any point between the current time and the last time.

According to the wear degradation law of self-lubricating bearings introduced in Section 2.2, this paper constructs a physical penalty term for the model, so that the model better conforms to physical laws during the learning process. The physical loss term can be constructed using the following formula:

$$\mathcal{L}_{\mathrm{PDE}} = \sum_{i=1}^{N} Re\,L\,u\left(\frac{\partial^2 x}{\partial t^2}\right) \tag{22}$$

where $\mathcal{L}_{\mathrm{PDE}}$ is physical loss function, $Re\,L\,u(\cdot)$ is activation function.

At the same time, the optimization objectives include data loss and monotonicity loss. In this study, cumulative damage model is introduced into the PINN, constructing a neuron operator with physical mechanism constraints. The cumulative damage model itself has the physical property of monotonic increase, which naturally ensures the physical plausibility of the predictions in the PINN's loss function without the need to add additional monotonicity constraints. Therefore, the remaining optimization objectives only need to be constructed for the data term, and its expression can be represented by the following formula. The total loss function is shown in Figure 7.

$$\mathcal{L}_{\mathrm{data}} = \frac{1}{n}\sum_{i=1}^{n}(y_i - \hat{y}_i)^2 \tag{23}$$

$$\mathcal{L} = \mathcal{L}_{\mathrm{data}} + \alpha\mathcal{L}_{\mathrm{PDE}} \tag{24}$$

where $\mathcal{L}_{\mathrm{data}}$ is the data loss function, y_i is the true value and $\hat{y}_i$ is the predicted value, α is trade-off parameters.

Journal of Computing and Information Science in Engineering. Received November 25, 2025;
Accepted manuscript posted February 19, 2026. doi:10.1115/1.4071182

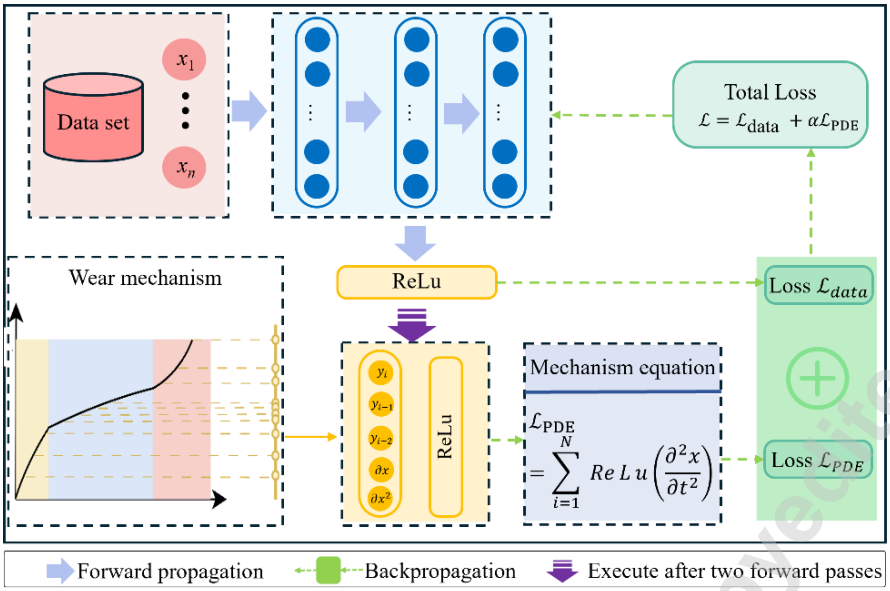

Figure 7. Physics-based constraint mechanism

4. Experimental case study

4.1 Experiment setup

To investigate the wear degradation behavior of self-lubricating bearings, a full life-cycle wear test platform was designed and constructed. As illustrated in Figure 8, the platform is primarily composed of four core parts: a loading system, a driving system, a control system, and a data acquisition network.

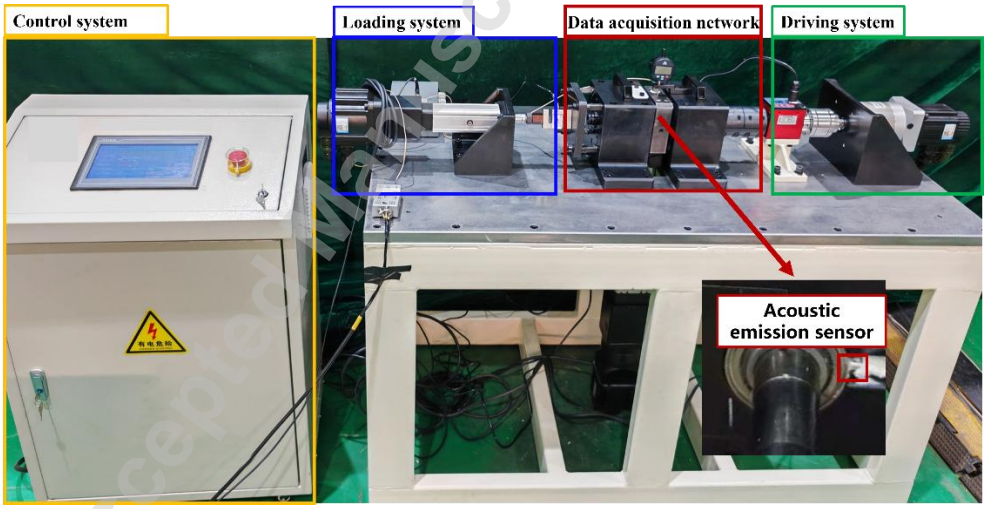

Figure 8. Full life cycle self-lubricating bearing wear experimental platform

To clearly illustrate the various components of the platform, Figure 9 shows the details of each component. Accurate and controllable loads, along with high-quality data acquisition, are crucial for predicting wear. So, the following sections will provide detailed explanation of the design schemes and key components of the subsystems.

Journal of Computing and Information Science in Engineering. Received November 25, 2025;
Accepted manuscript posted February 19, 2026. doi:10.1115/1.4071182

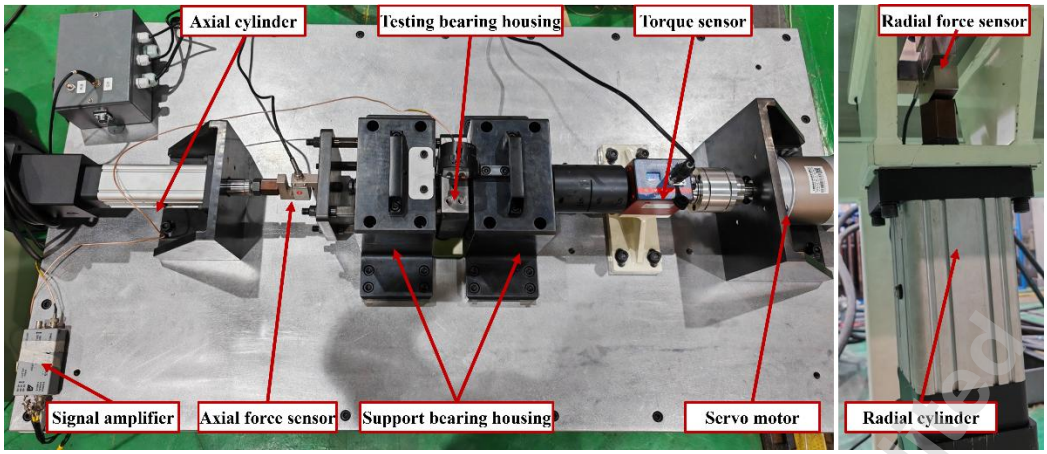

Figure 9. Detailed part of test platform for self-lubricating bearing

The loading system is designed to simulate the loads experienced by self-lubricating bearings during actual flight profiles. It consists of independent axial and radial loading modules, with a schematic diagram shown in Figure 10. Loading in both directions is driven by cylinders to achieve precise force control. Axial loading (Figure 10*a*): The axial cylinder produces tensile force by pulling the axial loading plate. One end of the loading rod is bolted to this pulling plate, while the other end passes through the support bearing housing and connects to the bearing under test. Through this force transmission path, the axial load is accurately applied to the bearing under test. Radial loading (Figure 10b): The radial cylinder acts directly on the bearing housing under test through a loading rod. The loading rod is bolted to the bearing housing, thereby applying the preset radial load to the bearing under test.

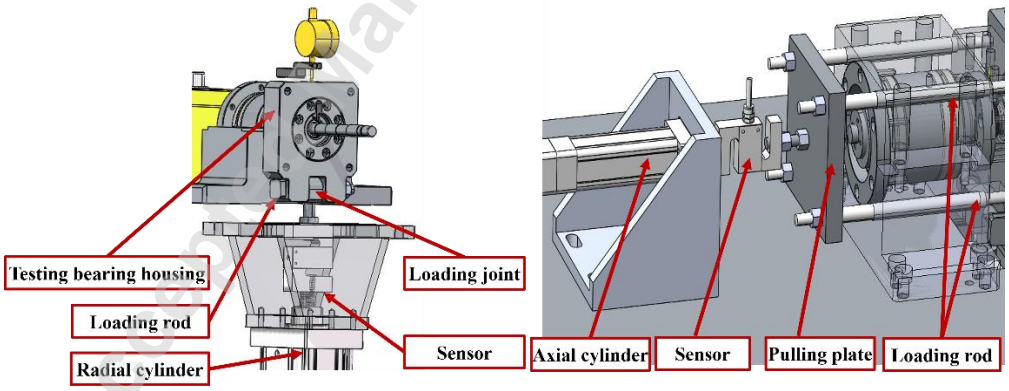

(*a*) Axial loadin (b) Radial loading

Figure 10. Load system diagram

The drive system is responsible for providing reciprocating oscillation for the test, and its structure is shown in Figure 11. The power transmission path of this system is as follows: the servo motor is coupled with a planetary gearbox to generate the set speed and to reduce speed while increasing torque. Subsequently, the reduced torque is

Journal of Computing and Information Science in Engineering. Received November 25, 2025;
Accepted manuscript posted February 19, 2026. doi:10.1115/1.4071182

transmitted to the torque sensor through a dual-disc coupling. Finally, the torque is transferred from the sensor to the rotating main shaft via a locking coupling, thereby driving the self-lubricating bearing specimen to perform reciprocating oscillation.

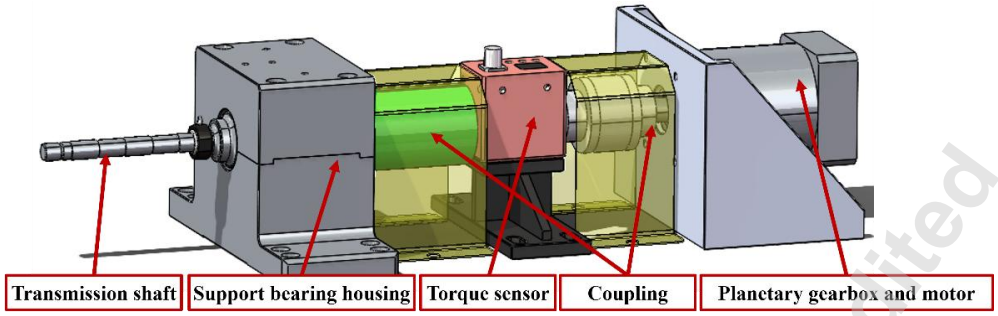

Figure 11. Drive system diagram

In the data acquisition network, special designs were made to ensure measurement accuracy. A high-precision displacement sensor is installed in a pre-drilled hole in the bearing housing, with its probe in contact with the bearing's outer ring for real-time, direct measurement of the radial displacement caused by wear, i.e., the wear depth. Simultaneously, an AE sensor is tightly coupled with the bearing's outer ring through a pre-set channel inside the housing to minimize signal attenuation, thereby acquiring high-fidelity AE signals. A schematic diagram of the system is shown in Figure 12.

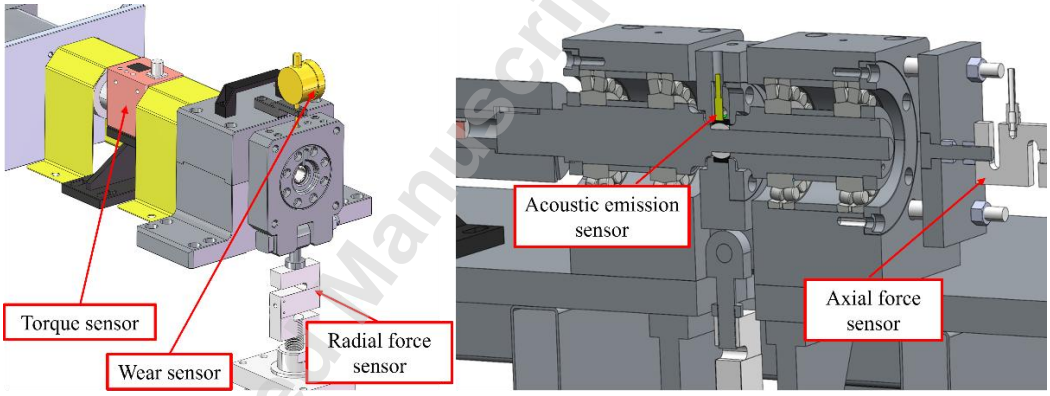

Figure 12. Data acquisition network diagram

The control system of the experimental platform adopts a hierarchical control architecture, with its system principle illustrated in Figure 13. The lower-level controller is a programmable logic controller (PLC), responsible for controlling the operation of the axial and radial cylinders. The upper-level controller is an industrial computer running a closed-loop feedback control algorithm. This algorithm compares the feedback signals from the sensors with predefined load/motion profiles in real time. When the deviation exceeds the threshold, the industrial computer generates compensation instructions sent to the PLC, which then drives the corresponding

actuators to make adjustments, ensuring the precise reproduction of test conditions. The main technical specifications of this test platform are detailed in Table 1.

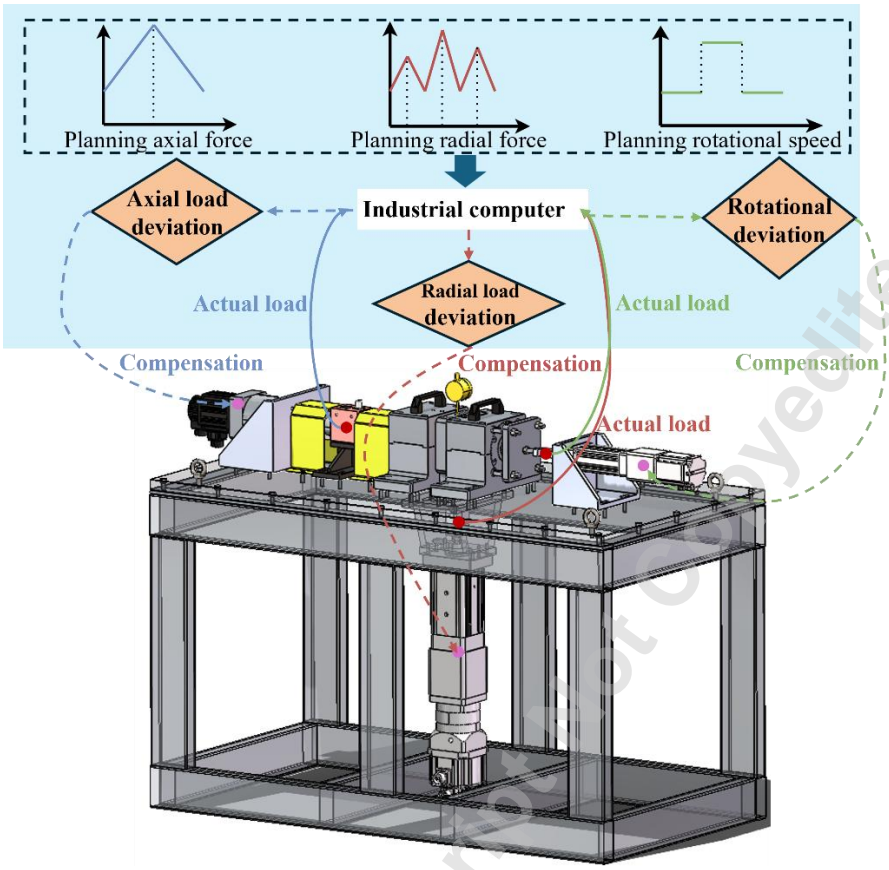

Figure 13. Designed test platform and dynamic load control

Table 1 Main technical specifications of test platform

Test platform component	Specification	Main parameters
Motor	ECMA-J11010RS	Power: 1000 W
Epicyclic gearbox	PLF-120	Maximum input speed: 4800r/min
Loading cylinder	YRJ065-L20-B5E-H3K1S3	/
PLC	LY-CS05	/
Wear sensor	SN-312-822	/
AE sensor	QC-MG500/1	Frequency domain: 100KHZ-1000KHZ

To rigorously validate the effectiveness and engineering practicality of the proposed PINN model, the experimental conditions in this study strictly simulated the actual operating conditions of an aircraft. During the experiment, all key parameters (such as load, swing frequency, and angle) were precisely controlled through a high-

Journal of Computing and Information Science in Engineering. Received November 25, 2025;
Accepted manuscript posted February 19, 2026. doi:10.1115/1.4071182

precision, closed-loop system integrated with the test platform's servo control system and PLC, in order to reproduce the actual application environment to the greatest extent possible. Crucially, to ensure the authenticity and representativeness of the data, full-life-cycle wear experiments were conducted. No form of accelerated aging was used, with the aim of obtaining the most genuine and un-manipulated wear evolution data of self-lubricating bearings under typical aviation operating conditions.

During the experiment, AE and wear data were acquired via a host computer. Specifically, AE signals were sampled at a high frequency of 2 MHz to finely record the bearing's state throughout the entire 110000-cycle operational period. Concurrently, wear data was acquired at a frequency of 20 Hz, covering the same cycle range.

4.2 Dataset preparation

To construct a benchmark dataset capable of effectively training and accurately evaluating proposed model, a systematic, physics-based data selection and alignment protocol was designed and executed. In fact, during long-term operation, elevated temperatures at the bearing contact interface significantly interfere with AE signal characteristics. To separate the effects of wear from thermal effects in analysis, the following strategy was adopted: each operational day was treated as an independent experimental unit, and only data from the after two hours after startup were selected. This period corresponds to the stage when the bearing reaches thermal stability, ensuring that all selected data points are obtained under isothermal conditions. Building on this foundation, precise feature-label pair construction was performed. For each selected 2-hour data segment, a representative, complete AE signal cycle was extracted as the input sample. In strict synchronization, wear measurement data within the same time window was extracted to serve as the corresponding supervised learning label for that AE sample. This one-to-one, time-synchronized pairing strategy ensures the causal relationship between input features and output labels, which is the cornerstone of building a high-quality predictive model. The detailed composition parameters of the final dataset are summarized in Table 2.

Table 2 Data set composition

Signal type	Sample frequency	Sampling period	Extraction time
AE	2 M HZ	full life circle	two hours later
Wear	20 HZ	full life circle	two hours later

4.3 Results and discussions

In this section, the proposed hybrid framework is employed to predict wear depth

in self-lubricating bearings. Concurrently, the predictive performance of the proposed model is compared with multiple alternative approaches, and the interpretability of the mechanism-fused model is further analyzed.

4.3.1 Evaluation index

Two metrics were constructed to evaluate the prediction results, including Mean Absolute Error (MAE) and Root Mean Square Error (RMSE). These metrics are widely used in existing prediction methods. The formulas for MAE and RMSE are as follows:

$$\mathrm{MAE} = \frac{1}{N}\sum_{i=1}^{N} |y_i - \hat{y}_i| \tag{25}$$

$$\mathrm{RMS} = \sqrt{\frac{1}{N}\sum_{i=1}^{N} (\hat{y}_i - y_i)^2} \tag{26}$$

4.3.2 Parameter establishment

Before training the model, it is necessary to provide the model with parameters of the physical model as well as hyperparameters of the neural network model, including the wear coefficient of the Archard model, the number of hidden layer neurons in the MLP model, the learning rate, and the dropout probability.

In the physical model, the K value is not a universal physical constant but a dimensionless, highly composite parameter that depends heavily on the material system and surface condition of the friction pair. Physically, it represents the probability of wear debris generation due to the interaction of asperities in a specific sliding contact. Therefore, accurately determining the wear coefficient K value is the fundamental prerequisite for ensuring the predictive accuracy of the Archard model and serves as a key bridge connecting theoretical models to actual wear behavior. Considering the material system of the self-lubricating bearing used in this study, the K value is 1.0452×10^{-10} mm²/N [5].

In deep learning models, predictive performance heavily depends on the proper setting of key hyperparameters. These parameters collectively determine the model's learning capacity, convergence speed, and generalization performance. The number of hidden layers and the number of neurons in each layer directly determine the model's complexity and fitting ability. To achieve a balance between model performance and computational efficiency, this study adopts a structure with 5 hidden layers. The learning rate is the core hyperparameter that controls the step size of weight updates

Journal of Computing and Information Science in Engineering. Received November 25, 2025;
Accepted manuscript posted February 19, 2026. doi:10.1115/1.4071182

during gradient descent. Considering both convergence efficiency and stability, this study sets the initial learning rate to 0.001. To further enhance the model's generalization ability and effectively suppress overfitting, this study introduces dropout regularization between hidden layers. Specifically, a dropout probability of 0.5 is applied, meaning that during training, each neuron in the hidden layers has a 50% chance of being temporarily ignored.

In summary, the selected values of physical parameters and hyperparameters are shown in Table 3.

Table 3 Hyperparameter settings

Hyperparameter	Value	Hyperparameter	Value
K	1.0452×10^{-10}	learning rate	0.001
Number of hidden layers	5	dropout probability	0.5

4.3.3 Model results and comparisons

This section systematically validates the superiority of proposed PINN model by benchmarking it against a multi-level matrix of comparison models. First, the comparative results of all models are presented collectively. Subsequently, detailed comparative results for each level are shown in subsequent subsections. The overall predicted trajectories are illustrated in Figure 14, while the error quantification results are presented in Figure 15.

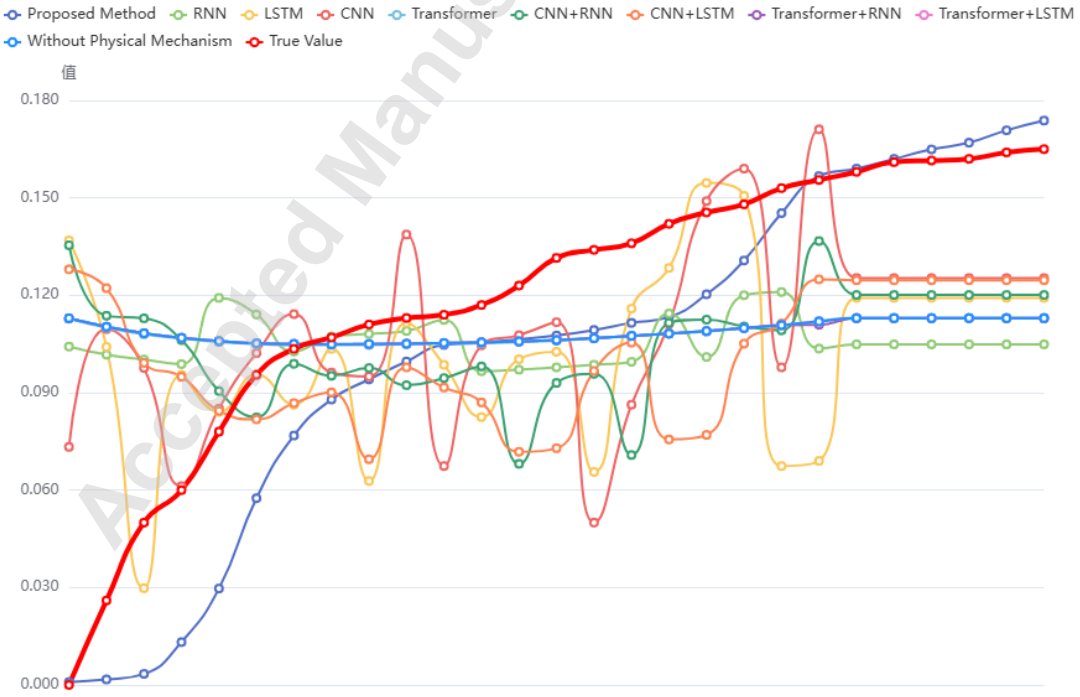

Figure 14. Performance comparison of different models

Journal of Computing and Information Science in Engineering. Received November 25, 2025;
Accepted manuscript posted February 19, 2026. doi:10.1115/1.4071182

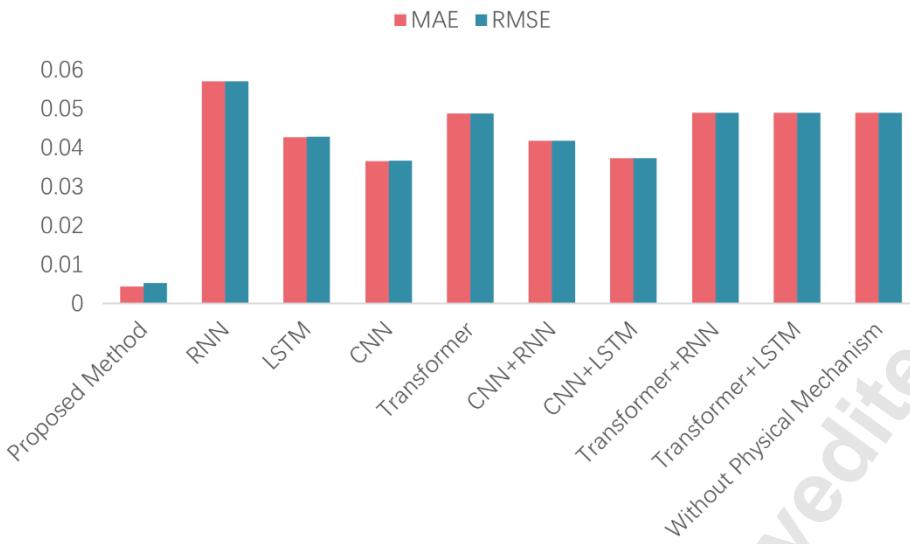

Figure 15. Comparison of prediction errors for different models

4.3.3.1 Compare with a single model

The wear process of bearings is essentially a time series problem. Therefore, several representative deep learning models that perform well in the field of time series prediction were selected as baseline references to evaluate their performance in directly predicting wear. For the single-model comparison, four highly representative deep learning models from the field of time series analysis were selected as baselines: RNN, LSTM, CNN, and Transformer models. The input for all these models was unified as the AE signal data processed by Compressed Sensing. Their common objective is to directly learn the complex non-linear mapping from the input signal to the final wear value of the self-lubricating bearing through end-to-end training.

Figure 16 illustrates the comparison between the predicted trajectories of the single model and the proposed model. When applied to the full-lifecycle data collected on-site, the first-category benchmark model exhibits overall poor predictive performance. As seen in Figure 16, the output of the Transformer model remained almost unchanged, while the CNN, LSTM, and RNN models, though exhibiting fluctuations, produced trajectories that were inconsistent with the actual wear trend. This is primarily because, during the long steady-state wear period, the actual change in wear amount is extremely slow and subtle, leading to a very low signal-to-noise ratio. Under these conditions, purely data-driven models struggle to learn the effective degradation law and are instead prone to interference from noise. In contrast, proposed PINN model, by embedding physical laws, is guided towards the correct function space, thus exhibiting superior prediction performance.

Journal of Computing and Information Science in Engineering. Received November 25, 2025;
Accepted manuscript posted February 19, 2026. doi:10.1115/1.4071182

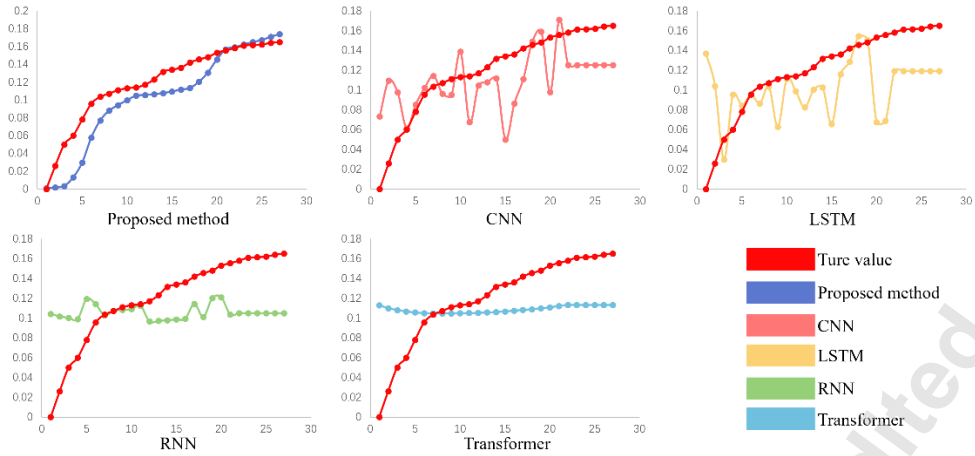

Figure 16. Comparison of prediction results for single model

4.3.3.2 Compare with hybrid models

To combine the strengths of different models, a hybrid model consisting of several deep learning models was constructed as the second type of comparison. The second comparison model adopted a "feature extractor-sequence processor" architecture. Specific combinations included CNN-LSTM, CNN-RNN, Transformer-LSTM, and Transformer-RNN. In this architecture, CNN or Transformer is first used for its powerful feature learning capability to extract deeper and more discriminative abstract features from the compressed sensing processed AE data. Subsequently, these feature sequences carrying key information are fed into sequence models such as LSTM or RNN for training, in order to capture the long-term temporal dependencies between features, ultimately obtaining more accurate predictions of self-lubricating bearings wear.

Figure 17 illustrates the comparison between the hybrid model and the proposed model's predicted trajectories. The second baseline model—the hybrid model—also failed to capture the correct wear pattern. Interestingly, the error comparison in Figure 17 shows that the performance of these hybrid models was even inferior to that of some single models. We speculate this may be because the feature extractor, when processing such slowly changing signals, acts as an information bottleneck, inadvertently discarding the subtle temporal information crucial for sequence modeling during the feature extraction process. This phenomenon further highlights the inherent limitations of purely data-driven models when data quality is constrained.

Journal of Computing and Information Science in Engineering. Received November 25, 2025;
Accepted manuscript posted February 19, 2026. doi:10.1115/1.4071182

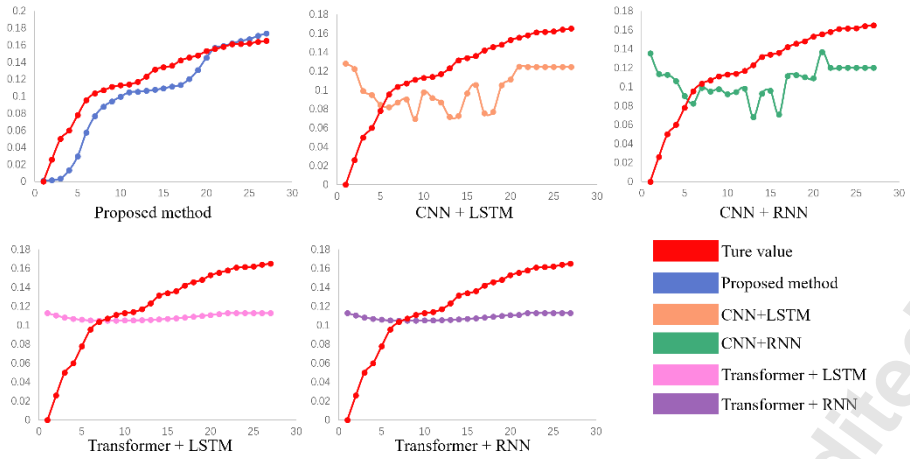

Figure 17. Comparison of prediction results for hybrid models

4.3.3.3 Compare with proposed model without physical mechanisms

The comparison between the proposed model and the model that does not incorporate physical mechanisms is shown in Figure 18. This model, which has an identical network architecture and hyperparameters to proposed PINN except for the removal of the "physics neuron operator" and physical loss constraints, performed similarly to the first and second classes of baselines and failed to capture the slow monotonic trend and yielded substantially larger errors. These results indicate that performance gains stem from the embedded physics rather than architecture alone.

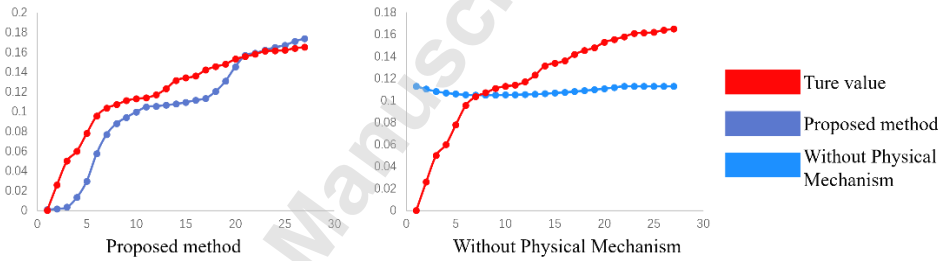

Figure 18. Comparison of prediction results for proposed model without physical mechanisms

4.3.4 Effectiveness of Physical Neural Networks

In this subsection, the role of embedding “physics neuron operator” in deep learning models is discussed from the perspectives of model interpretability and accuracy.

A truly interpretable predictive model should not only provide accurate results but also reveal the 'why' and 'how' behind those results. To this end, a dual-diagnostic framework is proposed to systematically evaluate the physical interpretability of the proposed model, transforming it from a “black box” into an analyzable “gray box.” First, deviation analysis of cumulative wear trajectories is conduct. Thanks to the

Journal of Computing and Information Science in Engineering. Received November 25, 2025;
Accepted manuscript posted February 19, 2026. doi:10.1115/1.4071182

embedded cumulative damage law in the model, the predicted trajectory can be compared and evaluated point by point against actual degradation data. This not only quantifies the overall prediction error, but more importantly, assesses whether the error sequence itself carries physical meaning. Second, instantaneous wear rates can be diagnosed. The designed "physics neuron operator" enables the instantaneous wear rate of computations within the network to be measured. By comparing the model's internal predicted values with the instantaneous wear rate derived from real data, the performance of the model at each time step can be accurately evaluated. Since the instantaneous wear rate is jointly determined by the data-driven component and the Archard physical model, analyzing the error in the instantaneous wear rate effectively quantifies the adaptive learning behavior of the data-driven component under physical constraints. This allows us to clearly identify, at every predicted moment, whether the data corrects the physical model or the physical model constrains the data, thereby achieving deep insights into the model's internal decision-making mechanisms.

Figure 19 displays the results for the cumulative wear trajectory deviation and the internal diagnosis of the instantaneous wear rate, respectively, to systematically evaluate the physical interpretability of the proposed model. Analysis of cumulative wear trajectory deviation (Figure 19 *a*) reveals significant error deviation during the initial stage, consistent with the inherent high uncertainty in the wear process at this phase [53,56,57]. Subsequently, the deviation decreases, which is attributable to the penalty on cumulative error in the loss function, reflecting the model's adaptive correction capability. Upon entering the steady-state wear period, the error does not vanish but instead fluctuates slowly within a bounded range. This smooth fluctuation, rather than sharp oscillations, is precisely because the embedded physical constraint for the wear stages acts as a regularizer, preventing the model from overfitting to local data points and compelling it to adhere to the macroscopic degradation law [40]. Crucially, the point of slope change (i.e., the inflection point) of the deviation curve has a clear physical meaning. As shown in Figure 19*a*, this inflection point occurs at the 7th monitoring point, which perfectly aligns with the critical point of transition from the running-in to the steady-state phase observed in the experiment. This provides compelling evidence that the model not only fitted the data but also autonomously learned and identified the physical phase transition point. In summary, by embedding "physics neuron operator" the model's prediction process can be "dissected," thereby significantly enhancing its reliability and controllability.

Journal of Computing and Information Science in Engineering. Received November 25, 2025;
Accepted manuscript posted February 19, 2026. doi:10.1115/1.4071182

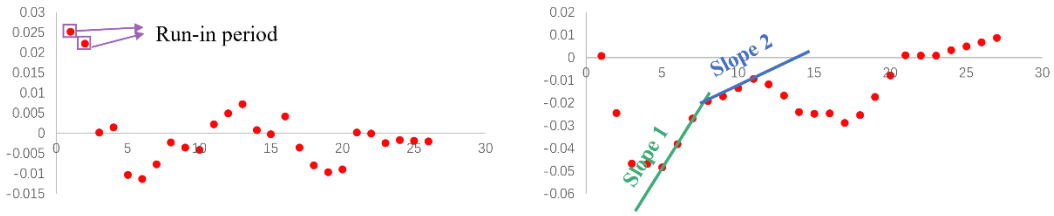

(*a*) (b)

Figure 19. Error of the proposed model. (*a*) Deviation results for cumulative wear trajectories (b) internal diagnostic results for instantaneous wear rates

For the internal diagnosis of the instantaneous wear rate, its visualization is shown in Figure 19b. In the initial running-in phase, the prediction error of the instantaneous wear is significantly high. This is mainly because, on a physical level, the running-in stage involves the fracture and plastic deformation of numerous asperities, causing the actual Archard wear coefficient to be a highly variable dynamic parameter [55]. However, the built-in Archard formula in proposed model uses a relatively simplified wear coefficient and thus cannot fully capture the high stochasticity of this stage, leading to the initial error. However, as the wear enters the stable stage, the prediction error rapidly converges and is maintained within a minimal range (± 0.01), exhibiting stable fluctuation. This phenomenon reveals the synergistic working mechanism within the model: on the one hand, the physical laws embedded in the loss function constrain the MLP's prediction of contact stress, preventing abrupt changes caused by data noise; on the other hand, the data-driven MLP module performs fine-tuning within the physical framework to adapt to changes in real operating conditions. This stable, low-error fluctuation, rather than zero error, also appropriately represents the inherent random uncertainty in wear prediction. In summary, the diagnostic results of the instantaneous wear rate indicate that proposed model successfully achieves an effective balance between adhering to dominant physical laws and adapting to dynamic data changes, thereby enabling reliable and accurate prediction of the subsequent stable wear stage.

In summary, the proposed model can effectively improve prediction accuracy. More importantly, it builds an intelligent prediction model with traceable mechanisms and understandable decision-making. Firstly, by embedding "physics neuron operator", it ensures that the logic of wear calculation is confined within the Archard physical framework. This means the model's output is no longer a number, but a result that can be verified and derived step by step through physical formulas [40]. Secondly, by

introducing a physical loss function, a 'guardrail' is set for the model's learning process, forcing it to discover and fit the invariant physical degradation patterns behind the data, rather than simply memorizing the noise and randomness of a specific dataset [48]. The combined effect of these two mechanisms transforms the deep learning model from an opaque 'black box' into an analyzable 'grey box', clearly revealing its decision-making process and greatly enhancing its credibility and reliability in practical engineering applications.

5. Conclusion

Deep learning models face limitations when processing field-collected industrial data due to their excessive reliance on data quality and “black box” characteristics. To address this issue, this paper proposes a hybrid physical damage neural network based on the wear stages of self-lubricating bearings and establishes a full-lifecycle experimental platform for validation. The main conclusions are as follows:

1) The proposed model successfully learns the underlying functional relationships from field data. By embedding physical prior knowledge, it effectively mitigates the negative impact of data quality on prediction results, achieving accurate wear prediction for self-lubricating bearings.

2) Unlike purely data-driven models, this model integrates the Archard wear theory and cumulative damage law, making its internal computational logic adhere to real physical mechanisms. This opens the "black box" of deep learning and significantly improves the model's interpretability.

3) By embedding the wear degradation law into the loss function, the model's learning process is subjected to strong physical constraints. This compels the model to discover and fit the invariant physical laws behind the data, rather than simply memorizing the noise of a specific dataset, fundamentally enhancing its generalization ability.

4) Compared to other models, the experimental results demonstrate that the proposed model can autonomously identify and accurately pinpoint the physical critical point of the transition from the running-in to the steady-state phase, and it reasonably represents the inherent random uncertainty in the wear process.

Future work will primarily focus on two directions: first, exploring the introduction of an adaptive wear coefficient into the model to further reduce the impact of non-steady-state factors like the running-in period on prediction accuracy; second,

extending the dynamic wear framework constructed in this paper to explore its application potential in a broader range of industrial scenarios.

Acknowledgments

This work was funded by National Natural Science Foundation of China (Grant No. 92467101, 52275499), and Open Fund of National Key Laboratory of Strength and Structural Integrity (No. LSSIKFJJ202402003).

References

[1] Xue, Y., 2026, "Research on the Influence of Microscale Aspheric Surface on the Contact and Wear Performances of Self-Lubricating Spherical Plain Bearing," ASME Journal of tribology, **148**(2), p. 021404. https://doi.org/10.1115/1.4068914.

[2] Lee, Y. J., Lee, K. H., and Lee, C. H., 2018, "Self-Lubricating and Friction Performance of a Three-Dimensional-Printed Journal Bearing," ASME Journal of tribology, **140**(5), p. 054501. https://doi.org/10.1115/1.4039995.

[3] Baş, H., and Karabacak, Y. E., 2023, "Prediction of Friction Coefficient and Torque in Self-Lubricating Polymer Radial Bearings Produced by Additive Manufacturing: A Machine Learning Approach," Proceedings of the Institution of Mechanical Engineers, Part J: Journal of Engineering Tribology, 237(11), pp. 2014–2038. https://doi.org/10.1177/13506501231196355.

[4] Li, J., Zhang, W., Tang, Z., Hu, T., Li, X., Wu, W., and Zhang, C., 2024, "Facile Fabrication and Tribological Properties of Self-Lubricating Polyurethane Based on Expanded Graphite/Paraffin for Water Lubricated Bearings," Journal of Materials Research and Technology, **33**, pp. 9791–9801. https://doi.org/10.1016/j.jmrt.2024.12.032.

[5] Zhang, Y. P., Shang, J. Z., Chen, Y., Zhang, C. H., and Wang, Y. S., 2013, " Wear-life Models for Self-Lubricating Spherical Plain Bearing, " Journal of National University of Defense Technology, **35**(6), pp.53-59.

[6] Qiu, M., Zhang, R., Li, Y. C., Du, H., and Pang, X. X., 2018, "Preparation and Tribological Properties of MoS2/Graphite Composite Coatings Modified by La2O3," Industrial Lubrication and Tribology, **70**(8), pp. 1422–1430. https://doi.org/10.1108/ILT-04-2017-0117.

[7] Liu, R., and Zhang, Y., 2024, "Study on the Tribological Performance of Self-Lubricating Thrust Ball Bearings with Different Embedded Features," ILT, **76**(6), pp. 822–831. https://doi.org/10.1108/ILT-03-2024-0073.

[8] Liu, C., Wang, J., Zhao, S., Yan, X., and Qi, X., 2023, "Influence of an Outer Ring End Offset on the Service Life and Eccentric Wear Defects of Self-Lubricating Spherical Plain Bearings," Engineering Failure Analysis, **143**, p. 106853. https://doi.org/10.1016/j.engfailanal.2022.106853.

[9] Zhang, Y., Zhang, T., Hui, L., An, J. L., and Qi, Y. M., 2026, "Accelerated Life Test Method for Low Speed Heavy Load Self Lubricating Joint Bearings," Tribology, **46**(2), pp. 1–9. DOI:10.16078/j.tribology.2024244.

[10] Deng, Y., Liu, L., Li, M., Jiang, M., Peng, B., and Yang, Y., 2023, "A Data-Driven Wheel Wear Prediction Model for Rail Train Based on LM-OMP-NARXNN," ASME Journal of Computing and Information Science in Engineering, **23**(2), p. 021012. https://doi.org/10.1115/1.4054488.

[11] Li, Z., Xiao, X., Zhou, W., Zhang, K., and Wang, W., 2025, "Prediction of Tool Wear by Improved Deep Belief Networks Based on Multi-Sensor Signals," ASME Journal of Computing and Information Science in Engineering, **25**(10), pp. 1–13. https://doi.org/10.1115/1.4069658.

[12] Lin, Y., Wang, H., Wang, H., Tang, S., Hao, H., and Huang, J., 2024, "A Novel Wear Prediction Method and Wear Characteristic Analysis of Piston/Cylinder Pair in Axial Piston Pump," Wear, **550–551**, p. 205402. https://doi.org/10.1016/j.wear.2024.205402.

[13] Xing, M., Liu, S., Cui, Y., Xu, J., Xu, Z., and Gao, L., 2024, "A Comprehensive Sliding Wear Prediction Method for Planetary Roller Screw Mechanism," Wear, **558–559**, p. 205536. https://doi.org/10.1016/j.wear.2024.205536.

[14] Zhang, A., Ni, J., Wei, X., Su, Y., and Liu, X., 2024, "A Tool Wear Prediction Method for Free-Form Surface Machining of Ball-End Mill," Journal of Manufacturing Processes, **130**, pp. 87–101. https://doi.org/10.1016/j.jmapro.2024.08.068.

[15] Li, D., Liu, X., Liao, H., Bing, L., Hou, P., Nie, R., and Jiao, Z., 2024, "A Prediction Model of Fluid–Solid Erosion Wear in Hydraulic Spool Valve Orifice," Wear, **540–541**, p. 205235. https://doi.org/10.1016/j.wear.2023.205235.

[16] Luo, L., Wang, X., Liu, H., and Zhu, L., 2019, "Number Simulation Analysis of Self-Lubricating Joint Bearing Liner Wear," Int J Interact Des Manuf, **13**(1), pp. 23–34. https://doi.org/10.1007/s12008-018-0471-y.

[17] Lu, J. J., Qu, M., and Li, Y. C., 2015, "Wear Life Models for Self-lubricating Radial Spherical Plain Bearings," Journal of Mechanical Engineering, **51**(11), pp. 56–63.

[18] Hao, X., Wang, S., Huo, P., and Pan, D., 2021, "Life Prediction of Heavy-Load Self-Lubricating Liners," Advances in Mechanical Engineering, **13**(2), p. 1687814021992155. https://doi.org/10.1177/1687814021992155.

[19] Li, J., Liu, J., Du, S., and Zhang, Y., 2022, "Friction and Abrasion Performance of Polytetrafluoroethylene/Kevlar Braided Liner Under Accelerated Life Tests," Journal of Materi Eng and Perform, **31**(7), pp. 5918–5926. https://doi.org/10.1007/s11665-022-06635-5.

[20] Du, S. C., Liu, T., Huang, D. L., and Li, G. L., 2017, "An Optimal Ensemble Empirical Mode Decomposition Method for Vibration Signal Decomposition," Journal of Vibration and Acoustics, **139**(3), p. 031003. https://doi.org/10.1115/1.4035480.

[21] Deng, Y. F., Du, S. C., Jiao, S. Y., Zhao, C., and Xie, Z. Y., 2020, "Prognostic Study of Ball Screws by Ensemble Data-Driven Particle Filters," Journal of Manufacturing Systems, **56**, pp. 359–372. https://doi.org/10.1016/j.jmsy.2020.06.009.

[22] Deng, Y. F., Huang, D. L., Du, S. C., Li, G. L., Zhao, C., and Lv, J., 2021, "A Double-Layer Attention Based Adversarial Network for Partial Transfer Learning in Machinery Fault Diagnosis," Computers in Industry, **127**, p. 103399. https://doi.org/10.1016/j.compind.2021.103399.

[23] Deng, Y. F., Du, S. C., Wang, D., Shao, Y. P., and Huang, D. L., 2023, "A Calibration-Based Hybrid Transfer Learning Framework for RUL Prediction of Rolling Bearing Across Different Machines," IEEE Trans. Instrum. Meas., **72**, pp. 1–15. https://doi.org/10.1109/TIM.2023.3260283.

[24] Deng, Y. F., Lv, J., Huang, D. L., and Du, S. C., 2023, "Combining the Theoretical Bound and Deep Adversarial Network for Machinery Open-Set Diagnosis Transfer," Neurocomputing, **548**, p. 126391. https://doi.org/10.1016/j.neucom.2023.126391.

[25] Jia, S. Y., Deng, Y. F., Lv, J., Du, S. C., and Xie, Z. Y., 2022, "Joint Distribution Adaptation with Diverse Feature Aggregation: A New Transfer Learning Framework for Bearing Diagnosis across Different Machines," Measurement, **187**,

p. 110332. https://doi.org/10.1016/j.measurement.2021.110332.

[26] Xie, Z. Y., Du, S. C., Lv, J., Deng, Y. F., Jia, S. Y., 2020, "A Hybrid Prognostics Deep Learning Model for Remaining Useful Life Prediction," Electronics, **10**(1). https://doi.org/10.3390/electronics10010039.

[27] Wang, Y. H., Wang, S., Du, S. C., Shen, X. X., Li, S. S., and Chen, X. M., 2025, "MTCAT: A Modern Temporal Convolution and Enhanced Attention Transformer Model for Remaining Useful Life Prediction of Aerospace Self-Lubricating Bearings," IEEE Sensors J., **25**(19), pp. 36513–36525. https://doi.org/10.1109/JSEN.2025.3597796.

[28] Yau, H. T., Kuo, P. H., and Hong, S. W., 2024, "Milling Wear Prediction Using an Artificial Neural Network Model," Engineering Applications of Artificial Intelligence, **135**, p. 108686. https://doi.org/10.1016/j.engappai.2024.108686.

[29] Li, Y., Huang, X., Tang, J., Li, S., and Ding, P., 2023, "A Steps-Ahead Tool Wear Prediction Method Based on Support Vector Regression and Particle Filtering," Measurement, **218**, p. 113237. https://doi.org/10.1016/j.measurement.2023.113237.

[30] Cheng, Y., Lu, M., Gai, X., Guan, R., Zhou, S., and Xue, J., 2024, "Research on Multi-Signal Milling Tool Wear Prediction Method Based on GAF-ResNext," Robotics and Computer-Integrated Manufacturing, **85**, p. 102634. https://doi.org/10.1016/j.rcim.2023.102634.

[31] Dong, J., Chen, T., Gao, Y., Su, D., and Jiang, H., 2024, "A Multi-Model Method for Tool Wear Prediction with Deep Temporal Features and Correlation Alignment," Meas. Sci. Technol., **35**(1), p. 015604. https://doi.org/10.1088/1361-6501/ad03b6.

[32] Pandiyan, V., Akeddar, M., Prost, J., Vorlaufer, G., Varga, M., and Wasmer, K., 2023, "Long Short-Term Memory Based Semi-Supervised Encoder—Decoder for Early Prediction of Failures in Self-Lubricating Bearings," Friction, **11**(1), pp. 109–124. https://doi.org/10.1007/s40544-021-0584-3.

[33] Hao, X., Wang, S., Huo, P., and Pan, D., 2021, "Life Prediction of Heavy-Load Self-Lubricating Liners," Advances in Mechanical Engineering, **13**(2), p. 1687814021992155. https://doi.org/10.1177/1687814021992155.

[34] Hao, X., Wang, S., Chen, M., and Pan, D., 2021, "Remaining Useful Life Prediction of High-Frequency Swing Self-Lubricating Liner," Shock and

Vibration, **2021**(1), p. 8843374. https://doi.org/10.1155/2021/8843374.

[35] Wang, X., Xiao, B., Zhang, B., Sun, R., Cui, L., and Liaw, P. K., 2025, "Deep Learning Applications in the Analysis of Wear Mechanisms in Metallic Materials: A Review," ACS Materials Lett., **7**(8), pp. 2936–2954. https://doi.org/10.1021/acsmaterialslett.5c00688.

[36] Cheng, Y., Hu, K., Wu, J., Zhu, H., and Shao, X., 2021, "A Convolutional Neural Network Based Degradation Indicator Construction and Health Prognosis Using Bidirectional Long Short-Term Memory Network for Rolling Bearings," Advanced Engineering Informatics, **48**, p. 101247. https://doi.org/10.1016/j.aei.2021.101247.

[37] Ferreira, C., and Gonçalves, G., 2022, "Remaining Useful Life Prediction and Challenges: A Literature Review on the Use of Machine Learning Methods," Journal of Manufacturing Systems, **63**, pp. 550–562. https://doi.org/10.1016/j.jmsy.2022.05.010.

[38] Afridi, Y. S., Hasan, L., Ullah, R., Ahmad, Z., and Kim, J. M., 2023, "LSTM-based Condition Monitoring and Fault Prognostics of Rolling Element Bearings Using Raw Vibrational Data," Machines, **11**(5). https://doi.org/10.3390/machines11050531.

[39] Li, X., Zhang, W., Ma, H., Luo, Z., and Li, X., 2020, "Data Alignments in Machinery Remaining Useful Life Prediction Using Deep Adversarial Neural Networks," Knowledge-Based Systems, **197**, p. 105843. https://doi.org/10.1016/j.knosys.2020.105843.

[40] Wang, S., Yan, L., Du, S. C., Li, S. S., and Chen, X. M., 2025, "Bearing Prognostics and Health Management Based on Hybrid Physical Mechanism and Data Models: A Systematic Review," Meas. Sci. Technol., **36**(5), p. 052002. https://doi.org/10.1088/1361-6501/adcce4.

[41] Pashmforoush, F., Ebrahimi Araghizad, A., and Budak, E., 2024, "Physics-Informed Tool Wear Prediction in Turning Process: A Thermo-Mechanical Wear-Included Force Model Integrated with Machine Learning," Journal of Manufacturing Systems, **77**, pp. 266–283. https://doi.org/10.1016/j.jmsy.2024.09.008.

[42] Li, Y., Wang, J., Huang, Z., and Gao, R. X., 2022, "Physics-Informed Meta Learning for Machining Tool Wear Prediction," Journal of Manufacturing

Systems, **62**, pp. 17–27. https://doi.org/10.1016/j.jmsy.2021.10.013.

[43] Gao, T., Zhu, H., Wu, J., Lu, Z., and Zhang, S., 2024, "Hybrid Physics Data-Driven Model-Based Fusion Framework for Machining Tool Wear Prediction," Int J Adv Manuf Technol, **132**(3–4), pp. 1481–1496. https://doi.org/10.1007/s00170-024-13365-6.

[44] Yuan, D., Luo, T., Zhang, D., and Zhu, K., 2023, "A Physics-Assisted Online Learning Method for Tool Wear Prediction," IEEE Trans. Instrum. Meas., **72**, pp. 1–11. https://doi.org/10.1109/TIM.2023.3273683.

[45] Zeng, Y., Chen, B., and Zhang, X., 2025, "Parameter Optimization of the Archard Model-Based Wheel Wear Prediction Using a Data-Driven Approach: Methodology and Verification," Wear, **578–579**, p. 206171. https://doi.org/10.1016/j.wear.2025.206171.

[46] Huang, W., Zhang, X., Wu, C., Cao, S., and Zhou, Q., 2022, "Tool Wear Prediction in Ultrasonic Vibration-Assisted Drilling of CFRP: A Hybrid Data-Driven Physics Model-Based Framework," Tribology International, **174**, p. 107755. https://doi.org/10.1016/j.triboint.2022.107755.

[47] Wang, J., Li, Y., Zhao, R., and Gao, R. X., 2020, "Physics Guided Neural Network for Machining Tool Wear Prediction," Journal of Manufacturing Systems, **57**, pp. 298–310. https://doi.org/10.1016/j.jmsy.2020.09.005.

[48] Li, H., Zhang, Z., Li, T., and Si, X., 2024, "A Review on Physics-Informed Data-Driven Remaining Useful Life Prediction: Challenges and Opportunities," Mechanical Systems and Signal Processing, **209**, p. 111120. https://doi.org/10.1016/j.ymssp.2024.111120.

[49] Zhang, H., Jiang, S., Gao, D., Sun, Y., and Bai, W., 2024, "A Review of Physics-Based, Data-Driven, and Hybrid Models for Tool Wear Monitoring," Machines, **12**(12), p. 833. https://doi.org/10.3390/machines12120833.

[50] Shannon, C. E., 1949, "Communication in the Presence of Noise," Proceedings of the IRE, **37**(1), pp. 10–21. https://doi.org/10.1109/JRPROC.1949.232969.

[51] Candes, E. J., Romberg, J., and Tao, T., 2006, "Robust Uncertainty Principles: Exact Signal Reconstruction from Highly Incomplete Frequency Information," IEEE Transactions on Information Theory, **52**(2), pp. 489–509. https://doi.org/10.1109/TIT.2005.862083.

[52] Hase, A., Mishina, H., and Wada, M., 2012, "Correlation between Features of Acoustic Emission Signals and Mechanical Wear Mechanisms," Wear, **292–293**, pp. 144–150. https://doi.org/10.1016/j.wear.2012.05.019.

[53] Liu, Y., Ma, G., Zhu, L., Han, C., Li, Z., Zhang, B., Zhao, H., Wang, H., and Chen, S., 2024, "A New Coated Self-Lubricating Spherical Plain Bearing with High Performance and Excellent Security," Proceedings of the Institution of Mechanical Engineers, Part J: Journal of Engineering Tribology, **238**(1), pp. 60–72. https://doi.org/10.1177/13506501231203034.

[54] Zong, F., Yang, X., Tan, D., Ye, Q., Hu, Y., He, Q., Yang, W., and Gao, H., 2023, "Influence of MoS_2 Coating Treatment on the Damage Behaviour of the Self-Lubricating Friction Pair of Spherical Plain Bearings," Proceedings of the Institution of Mechanical Engineers, Part J: Journal of Engineering Tribology, **237**(11), pp. 2138–2149. https://doi.org/10.1177/13506501231201689.

[55] Zhu, C., Chen, Q., and Liu, X., 2025, "Review of Advanced Fabric Composite Liners for Enhancing Tribological Performance on Self-Lubricating Joint Bearings," Surf. Sci. Technol., **3**(1), p. 4. https://doi.org/10.1007/s44251-024-00068-z.

[56] Chen, C., Yang, Q., Chen, Q., Wang, Y., Xu, D., Li, H., Zhang, X., Harvey, C. M., and Liu, J., 2022, "Tribological Properties of Copper-Embedded Self-Lubricating Bearing Materials," ILT, **74**(7), pp. 796–803. https://doi.org/10.1108/ILT-03-2022-0067.

[57] Han, C. H., Shi, J. D., Liu, Y. F., Liu, Q., Ma, G. Z., Li, G. L., and Wang, H.D., 2021, "Research Progress of Tribological Properties and Life Estimation Methods of Self-Lubricating Spherical Plain Bearings," Materials Reports, **35**(5), pp. 5166–5173.

[58] Yan, J., Jin, L., Yuan, Z., and Liu, Z., 2022, "RNN for Receding Horizon Control of Redundant Robot Manipulators," IEEE Trans. Ind. Electron., **69**(2), pp. 1608–1619. https://doi.org/10.1109/TIE.2021.3062257.

[59] Amalou, I., Mouhni, N., and Abdali, A., 2022, "Multivariate Time Series Prediction by RNN Architectures for Energy Consumption Forecasting," Energy Reports, **8**, pp. 1084–1091. https://doi.org/10.1016/j.egyr.2022.07.139.